Numerical and Experimental Analysis of the Motion of a Hyperelastic Body in a Fluid

Hamed Esmailzadeh[1], Mohammad Passandideh-Fard[2]

[1]Graduate Student, Ferdowsi University of Mashhad; esmailzadeh_hamed@yahoo.com
[2]Associate Professor, Ferdowsi University of Mashhad; mpfard@um.ac.ir

Abstract

In this study, a numerical algorithm is developed for simulating the interaction between a fluid and a 2D/axisymmetric hyperelastic body based on a full Eulerian fluid-structure interaction (FSI) method. In this method, the solid volume fraction is used for describing the multi component material and the deformation tensor for describing the deformation of the hyperelastic body. The constitutive law in the Cauchy stress form and an equation are used for the transport of the deformation tensor field which are the core elements of the simulation method. For materials with a low stiffness, an explicit formulation is used for the elastic stress. In some cases, however, due to high stiffness a semi implicit formulation is used for the elastic stress to avoid instability. The strain rate has a discontinuity across the fluid-body interface. For improving accuracy in capturing the interface, solid is treated as a highly viscous fluid. An experimental setup is used to validate the numerical results. The movement of a sphere made of silicone in air and its impact on a rigid surface are investigated. A high speed Charge-Coupled Device (CCD) camera is used to capture images and image processing techniques are employed to obtain the required data from images. For all cases considered, the results are in good agreement with those of the experiment performed in this study and other numerical results reported in the literature.

Keywords: Fluid Solid Interaction, Hyperelastic Material, Implicit Elastic Term, Image Processing

Introduction

Numerical methods for solving the fluid-structure interaction are classified in three major methods: Lagrangian-Lagrangian, Eulerian-Lagrangian and Eulerian-Eulerian. In the Lagrangian-Lagrangian method, a structured grid for the fluid and an unstructured grid for the solid are used. The computation is done with a moving mesh updated based on a method known as ALE (Arbitrary Lagrangian-Eulerian) [1-2]. In the Eulerian-Lagrangian method, however, an Eulerian background mesh is used for the fluid and a Lagrangian moving mesh for the solid. A number of these methods have been proposed by many researchers such as Gilmanov et al. [3] who introduced the hybrid immersed boundary method; Huang et al. [4] and Wang et al. [5-6] who proposed the immersed boundary method; and Glowinski et al. [7] who introduced the fictitious domain method. In the Eulerian-Eulerian method, a fixed mesh grid is used for both fluid and solid. Recently, Sugiyama et al. [8] used a FSI model based on an Eulerian framework for an incompressible fluid and a hyperelastic solid. They used this model to simulate biconcave neo-Hookean particles in a Poiseuille flow. They improved the model in later publications [9-14].

In the present study, a numerical method is developed based on the FSI model of Sugiyama et al. [9]. This method is capable of handling unprescribed motion of the solid. The method of Ii et al. [10] is used for elastic stress in order to simulate materials with high stiffness. They used a fourth-order Jacobian tensor to overcome the difficulty associated with the difference between the constitutive laws of solid and fluid. For improving the dynamic condition of the interface, high viscosity method is used for the solid. All the basic equations are numerically solved on a fixed Cartesian grid using a finite difference scheme. In the method of Sugiyama et al. [9], the fifth-order Weighted Essentially Non-Oscillatory (WENO) method is used to advect the solid volume fraction field, which temporally makes the interface numerically diffusive. In this paper, however, the Youngs Piecewise Linear Interface Calculation (PLIC) algorithm [15] is used that suppresses the numerical diffusion; this algorithm is frequently used in the multiphase flow simulations [16].

The present study also deals with the experimental characterization of silicone as a hyperelastic body. The neo-Hookean constitutive equation for this purpose is used based on the Marckmann et al. [17]. The neo-Hookean model is used for small deformation that involves only one material parameter and is able to predict the material response for different types of loading conditions.

Numerical Method

The following equations over the entire domain including both fluid and solid are solved:

$$\nabla \cdot V = 0 \qquad (1)$$

$$\frac{\partial V}{\partial t} + V \cdot \nabla V = \frac{-\nabla P}{\rho} + \frac{1}{\rho} \nabla \cdot \mu \left[(\nabla V) + (\nabla V)^T \right]$$
$$+ \frac{\nabla \cdot \tau_e}{\rho} + g \qquad (2)$$

where V is the velocity vector, ρ the density, P the pressure, μ the dynamic viscosity and g the acceleration due to gravity. The solid body is treated as a fluid with high viscosity. The solid volume fraction is advected using the VOF method by means of a scalar field ϕ, defined as:

$$\phi = \begin{cases} 0 & \text{in fluid} \\ 0<,<1 & \text{in fluid-solid interface} \\ 1 & \text{in solid} \end{cases} \qquad (3)$$

The discontinuity in ϕ is a lagrangian invariant, propagating according to:

$$\frac{D\phi}{Dt} = \frac{\partial \phi}{\partial t} + V \cdot \nabla \phi = 0 \qquad (4)$$

The density and viscosity in each cell are defined as:

$$\rho = (1-\phi)\rho_l + \phi\rho_s \qquad (5)$$

$$\mu = (1-\phi)\mu_l + \phi\mu_s \qquad (6)$$

The subscripts l and s stand for the fluid and solid phases, respectively.

The neo-Hookean model [8] gives the expression of the hyperelastic stress as:

$$\tau_e = 2C_1 B \qquad (7)$$

where the coefficient c_1 is determined experimentally. The deformation tensor B is temporally updated on a fixed mesh from the transport equation as:

$$\frac{\partial B}{\partial t} + V \cdot \nabla B = \nabla V^T \cdot B + B \cdot \nabla V \qquad (8)$$

with the initial stretch-free condition $B(t_0) = I$.

The second-order Adams-Bashforth scheme [9] is applied to update the variable B explicitly at the $(n+1)$th time level from the nth and $(n-1)$th time levels as:

$$B^{n+1} = B^n - \Delta t \{ \frac{3}{2} V^n \cdot \nabla B^n - \frac{1}{2} V^{(n-1)} \cdot \nabla B^{(n-1)}$$
$$- \frac{3}{2}(\nabla V^T \cdot B + B \cdot \nabla V)^n + \frac{1}{2}(\nabla V^T \cdot B + B \cdot \nabla V)^{(n-1)} \} \qquad (9)$$

As mentioned before, a semi implicit formulation is used to avoid instability due to high stiffness. So the method described in Ii et al. [10] is used for calculating the elastic term. For this purpose, four step projection method is developed. This method is an extension of the three-step projection method [16]. In the first step, the convective term and gravity are discretized using an explicit scheme. In the second step, the viscous term is discretized with a semi-implicit scheme. In the third step, the elastic term is discretized with a semi-implicit scheme that is the core element of this method. In the fourth step, the velocity field is projected on to a zero divergence vector field. This method is as follows:

$$\frac{V^{n+\frac{1}{4}} - V^n}{\Delta t} = -(V \cdot \nabla V)^n + g^n \qquad (10)$$

$$\frac{V^{n+\frac{2}{4}} - V^{n+\frac{1}{4}}}{\Delta t} = \frac{1}{\rho} \nabla \cdot \mu \left[\left(\nabla V^{n+\frac{2}{4}} \right) + \left(\nabla V^{n+\frac{2}{4}} \right)^T \right] \qquad (11)$$

$$\frac{V^{n+\frac{3}{4}} - V^{n+\frac{2}{4}}}{\Delta t} = \frac{\nabla \cdot \tau_e^{n+\frac{3}{4}}}{\rho} \qquad (12)$$

$$\frac{V^{n+1} - V^{n+\frac{3}{4}}}{\Delta t} = -\frac{\nabla p^{n+1}}{\rho} \qquad (13)$$

Ii et al. [10] rewrote Eq. 12 as:

$$\frac{V^{n+\frac{3}{4}} - V^{n+\frac{2}{4}}}{\Delta t} = \frac{1}{2} \nabla \cdot \left(\frac{\tau_e^{n+\frac{2}{4}} + \tau_e^{n+\frac{3}{4}}}{\rho} \right) \qquad (14)$$

The elastic stress $\tau_e^{n+\frac{3}{4}}$ is evaluated by introducing the fourth-order Jacobian tensor $J(B) = \frac{\partial \tau_e(B)}{\partial B}$ as:

$$\tau_e^{n+\frac{3}{4}} = \tau_e^{n+\frac{2}{4}} + J^{n+\frac{2}{4}} : \Delta B^{n+\frac{2}{4}} \qquad (15)$$

For evaluating the right hand side of Eq. 14, the $B^{n+\frac{2}{4}}$ is obtained via transport equation as:

$$\frac{B^{n+\frac{2}{4}} - B^n}{\Delta t} + \frac{3}{2} V^n \cdot \nabla B^n - \frac{1}{2} V^{n-1} \cdot \nabla B^{n-1}$$
$$= \frac{1}{2} \left(\nabla V^{(n)T} + \nabla V^{(n+\frac{2}{4})T} \right) \cdot B^n + \frac{1}{2} B^n \cdot \left(\nabla V^n + \nabla V^{n+\frac{2}{4}} \right) \qquad (16)$$

Based on the transport equation, $\Delta B^{n+\frac{2}{4}}$ is given by:

$$\Delta B^{n+\frac{2}{4}} = B^{n+\frac{3}{4}} - B^{n+\frac{2}{4}} = \frac{\Delta t}{2} [\left(\nabla V^{\left(n+\frac{3}{4}\right)T} - \nabla V^{\left(n+\frac{2}{4}\right)T} \right) \cdot B^n$$
$$+ B^n \cdot \left(\nabla V^{n+\frac{3}{4}} - \nabla V^{n+\frac{2}{4}} \right)] \qquad (17)$$

By substituting Eq. 15 and 17 in Eq. 14, a linear system for $V^{n+\frac{3}{4}}$ is given as:

$$\rho \frac{V^{n+\frac{3}{4}}}{\Delta t} - \nabla \cdot \left(\frac{\Delta t}{4} H \left(V^{\left(n+\frac{3}{4}\right)}, B^{(n)}, J^{\left(n+\frac{2}{4}\right)} \right) \right) = \rho \frac{V^{n+\frac{2}{4}}}{\Delta t}$$
$$- \nabla \cdot \left(\frac{\Delta t}{4} H \left(V^{\left(n+\frac{2}{4}\right)}, B^{(n)}, J^{\left(n+\frac{2}{4}\right)} \right) \right) + \nabla \cdot \tau_e^{\left(n+\frac{2}{4}\right)} \qquad (18)$$

where

$$H(V, B, J) = J : \left(\nabla V^T \cdot B + B \cdot \nabla V \right) \qquad (19)$$

To solve the resulted system of equations, Tri Diagonal Matrix Algorithm (TDMA) solver was used to obtain $V^{n+\frac{3}{4}}$. Using $V^{n+\frac{3}{4}}$ and Eq. 17, the intermediate deformation tensor $B^{n+\frac{3}{4}}$ is obtained. Using $B^{n+\frac{3}{4}}$ and regarding Eq.13, we can obtain B^{n+1} as:

$$B^{(n+1)} = B^{\left(n+\frac{3}{4}\right)} - \frac{\Delta t^2}{2} \left(\nabla \left(\frac{\nabla P^{n+1}}{\rho} \right)^T \cdot B^n + B^n \cdot \nabla \left(\frac{\nabla P^{n+1}}{\rho} \right) \right) \qquad (20)$$

Experimental Setup

To validate the numerical results, an experimental setup for the impact of a hyperelastic solid body with a rigid surface is used. A sphere made of silicone as a hyperelastic material, moves in air and impacts on a rigid surface; it then bounces back and moves upward. A high speed CCD camera, Grasshopper model, made in Point Grey Company, was used for taking images. Fig. 1 shows the schematic of experimental setup. The MATLAB software is employed for image processing and the required information obtained from the images with a numerical code written in this software. First, an image involving a calibration piece with known dimension is utilized for calibration. In this way, we can

find the scale factor for all images. Next, we perform image processing for these images and obtain the position and velocity of center of volume.
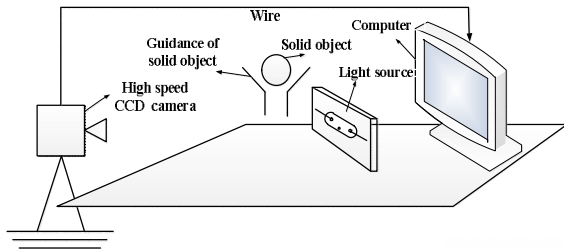

Figure 1. Schematic of experimental setup.

Numerical Results

In this section, numerical results of a few sample cases are presented. To validate the numerical model, we simulate the deformation of a number of cases for which the numerical results of other researchers are available in the literature. These cases include a soft wall deformed by a fluid flow as Wang et al. [5], a deformable solid motion in a lid-driven cavity with the same conditions as Sugiyama et al. [9] and an oscillating soft disk surrounded by a fluid as Robinson et al. [18]. Next, the numerical and experimental results of a bouncing of a hyperelastic sphere are presented.

-The deformation of a soft wall by fluid flow

The cavity considered is 2m by 2m, with bottom 0.5m occupied by a neo-Hookean wall and the upper part filled with a fluid. The velocities are zero at all cavity boundaries except the top lid, where the x component of the velocity is

$$u = 0.5 \begin{cases} \sin^2\left(\dfrac{\pi x}{0.6}\right) & x \in [0.0, 0.3) \\ 1 & x \in [0.3, 1.7] \\ \sin^2\left(\dfrac{\pi(x-2)}{0.6}\right) & x \in (1.7, 2.0] \end{cases} \quad (21)$$

The fluid and solid densities are assumed the same equal to $\rho_l = \rho_s = 1$. The viscosity is also assumed equal to $\mu_l = 0.2$. The coefficient of the elastic stress for the solid is $C_1 = 0.1$. The advection terms in the Navier-Stokes equation are omitted as in Wang et al [5]. The deformed wall reaches a steady state at $t = 8s$, when a
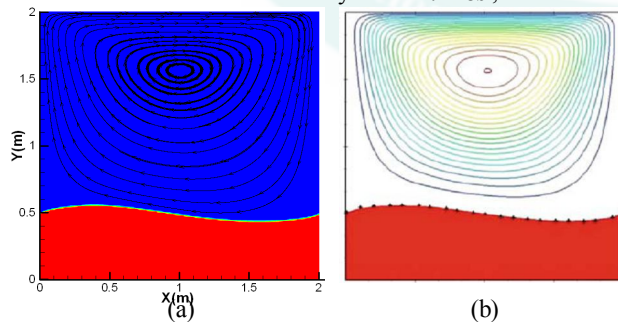

Figure2. The simulation results for a soft wall in a lid-driven cavity flow from a) present study and b) those of Wang et al. [5].

vortex is formed in the middle of the fluid domain. The wall deformation and the streamlines shown in Fig. 2

reveals a good agreement with those reported by Wang et al. [5].

-A solid motion in a lid-driven cavity flow

We perform simulation of deformable solid motion in a lid-driven cavity with the same setup and conditions as Sugiyama et al. [9]. The size of the cavity is 1m×1m. Initially the system is at rest. The unstressed solid shape is circular with a radius of 0.2m and centered at (0.6m, 0.5m). At $t = 0$, to drive the fluid and solid motions, the top wall starts to move at a speed of
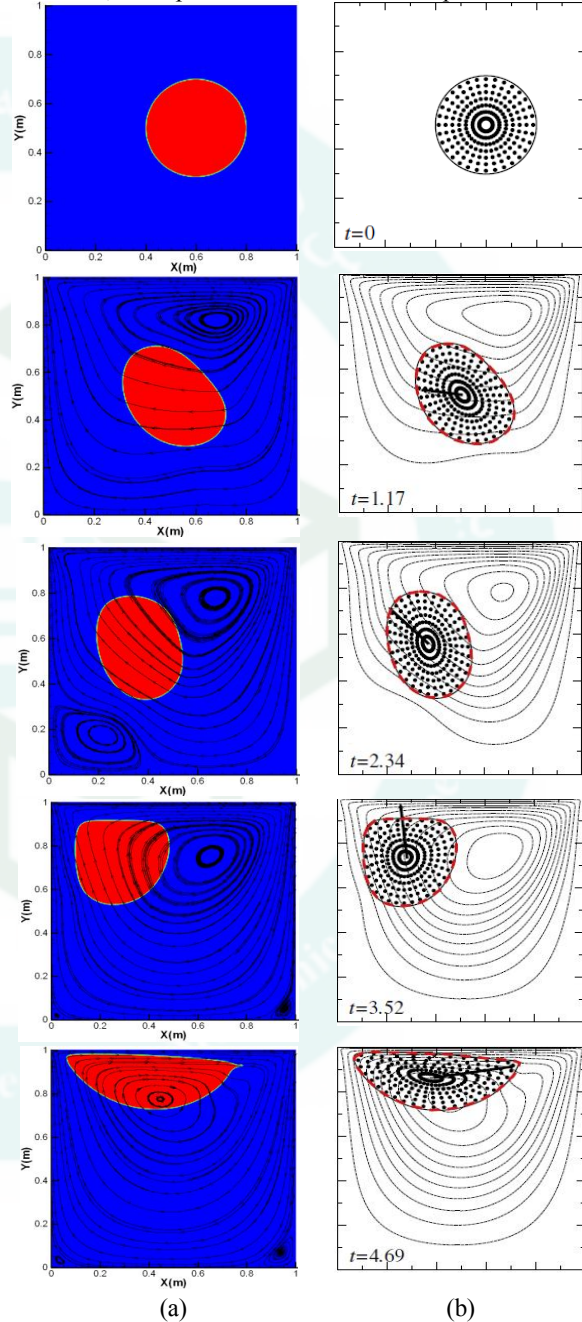

(a)   (b)

Figure3. The simulation results for a deformable solid motion in a lid-driven cavity flow from a) present study and b) those of Sugiyama et al. [9].

$V_{wall} = 1\dfrac{m}{s}$ in x direction. The no-slip condition is imposed on the walls. The solid component is neo-

Hookean material. The material properties are $\rho_l = \rho_s = 1$, $\mu_l = 0.01$ and $C_1 = 0.05$. The particle moves and deforms driven by the fluid flow and exhibits highly deformed shape, when the particle approaches the top wall. The deformation of the particle and the streamlines shown in Fig. 3 shows a good agreement with those reported by Sugiyama et al [9].

-Oscillating disk
We implement the oscillating disk example considered by Robinson et al. [18], where a circular deformable body is placed within a fluid domain of dimensions 1m×1m with no slip boundary conditions. An initial velocity is imposed in both the fluid and solid body based on the stream function $\psi = 0.05 \sin(2\pi x) \sin(2\pi y)$. We use a neo-Hookean constitutive model as described in [8] for the structure with $C_1 = 0.5$. The fluid and solid densities and viscosity are $\mu_l = 0.001$ and $\rho_l = \rho_s = 1$.

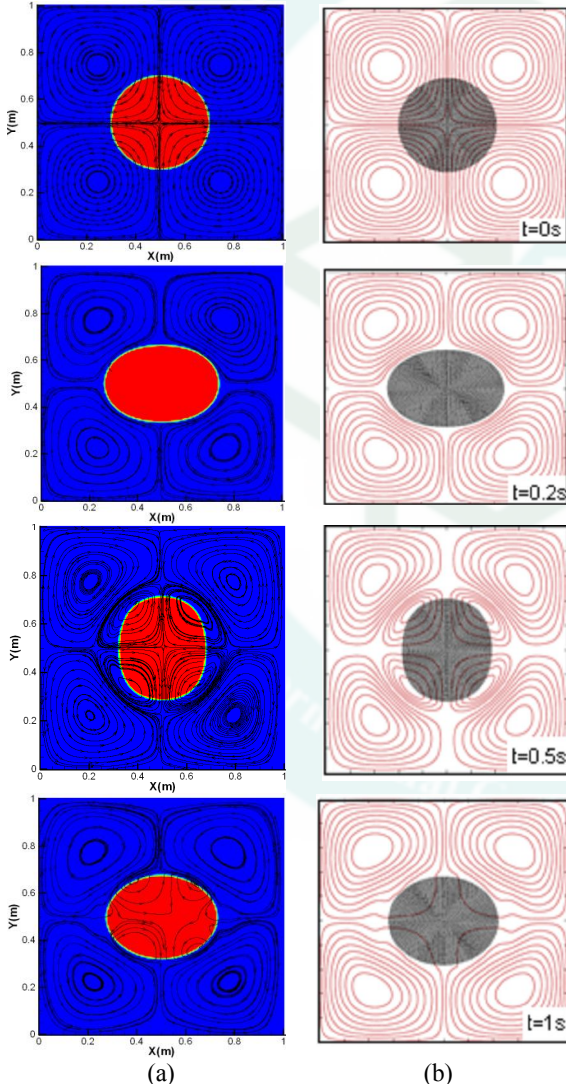(a)   (b)

Figure 4. The simulation results for an oscillating disk in fluid from a) present study and b) those of Robinson et al. [18].

The simulations are run for a period of 1s. The disk is initially stressed free and its undeformed shape is a

circle. At $t = 0.2s$, the maximum deformation is occurred. The vortices are seen in both fluid and solid at $t = 0.5s$. After this time, however, these vortices decay in the solid until $t = 1s$. Fig. 4 shows a good agreement between the results of the present study with those reported by Robinson et al. [18].

-Bouncing of a hyperelastic sphere on a rigid surface
A sphere made of silicone moves in air and hits with a rigid surface. A schematic of the problem and its initial condition considered for simulations are shown in Fig5.
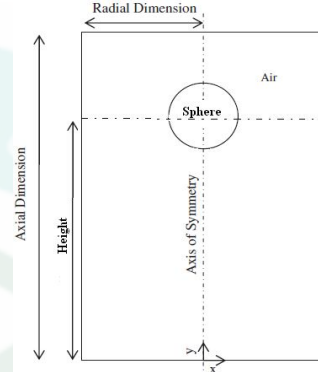

Figure 5. Schematic of a sphere during its motion in air and the initial and boundary conditions for the simulation.

The initial conditions and the properties are as follows:
Sphere radius: 1.92 cm
Initial position of sphere: 5.73 cm
Initial velocity of sphere: 1.22 $\frac{m}{s}$

Solid density: 1106 $\frac{kg}{m^3}$

The computational domain: 45mm×90mm (radius × height).
In Fig. 6, the numerical and experimental results for the evolution of the y-coordinate of the center of volume are shown. Also, Fig. 7 shows the velocity of the center of volume of sphere. Fig. 8 shows the numerical and experimental results of sphere before, during and after the impact. Particulary, the results were investigated during impact. By comparison of numerical and experimental results, the unknown coefficients of solid are found to be: $C_1 = 0.09$ Mpa and $\mu_s = 15 \frac{N.s}{m^2}$.

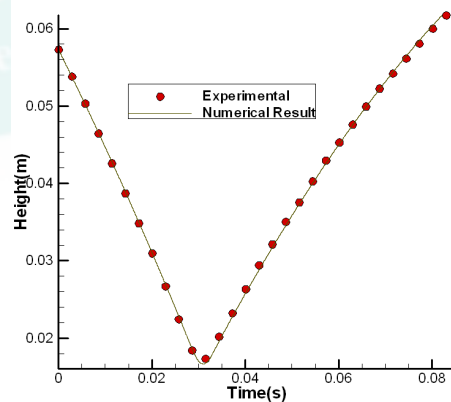Figure 6. Comparison of the numerical simulation results with experimental results of the y-coordinate center of volume.
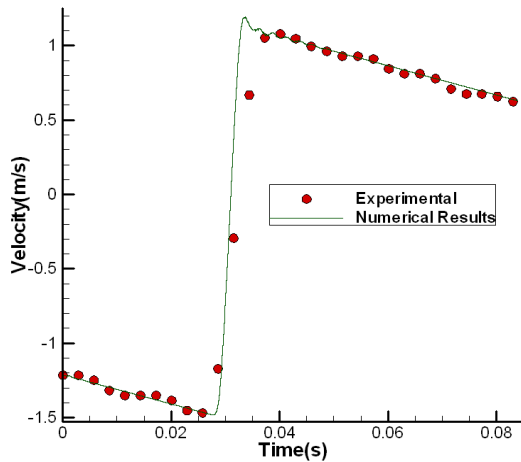
ISME2013, 7-9 May, 2013

Figure 7. Comparison of the numerical simulation results with experimental results of the velocity center of volume.

Fig. 9 shows the streamlines and the y-direction velocity contour in the computational domain at $t = 30.9\text{ ms}$, respectively. At $t = 30.9\text{ ms}$ the solid has reached almost a zero velocity.
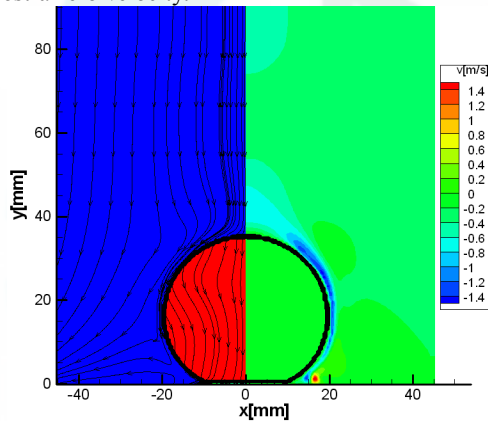

Figure 9. The streamline (left) and the y-direction velocity contour (right) at $t = 30.9\text{ ms}$.

To verify the validity of the obtained coefficients, other tests with different initial velocities and positions of
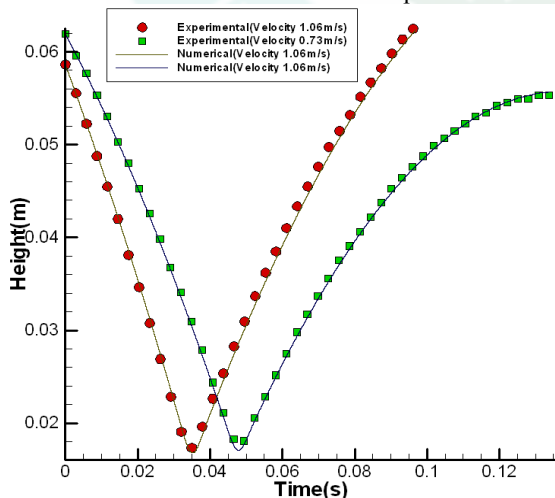

Figure 10. Comparison of the numerical simulation results with experimental results of the y-coordinate center of volume for initial velocities of solid.

sphere are performed using the same coefficients in the numerical program. As Figures 10 and 11 show, the numerical and experimental results well agree with each other for all cases.
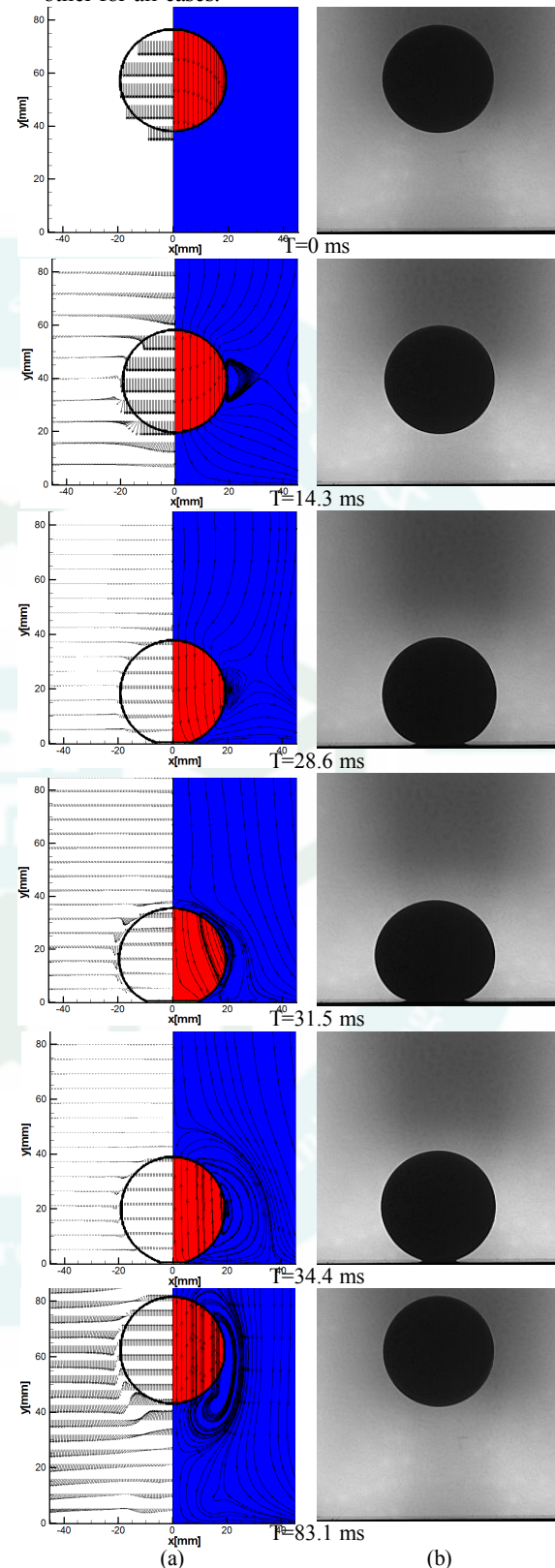

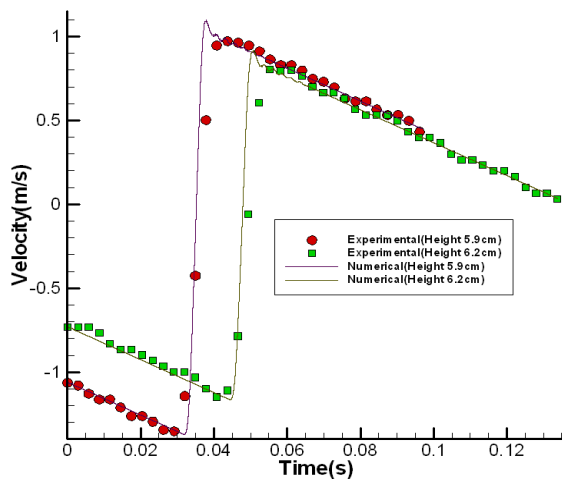Figure 8. Comparison of a) the numerical simulationresults with b) experimental results.

Figure 11. Comparison of the numerical simulation results with experimental results of the velocity center of volume for initial positions of solid.

Conclusions

A full Eulerian simulation method for solving fluid structure interaction (FSI) problems was developed. A VOF method was used to describe the multi component geometry. The temporal change in solid deformation was calculated in an Eulerian frame by updating a deformation tensor. An explicit formulation was utilized for the elastic stress. In high stiffness coefficients, an implicit formulation was used through a fourth-order Jacobian tensor to avoid the instability. For improving the dynamic condition in the fluid/solid interface, the high viscosity method was used for the solid region. As a result, the developed model was used for the deformation of a soft wall by fluid flow, the movement of a solid in a lid-driven cavity and an oscillating soft disk surrounded by a fluid. Also, the developed model was proven to be robust via experimental results. For this purpose, the movement of a sphere made of silicone in air and its impact on a rigid surface are investigated. Numerical results agreed well with those of the experiments and other available data in the literature.

References

[1] Hirt, C., Amsden, A., and Cook, J., 1974. "An arbitrary Lagrangian-Eulerian computing method for all flow speeds". *Journal of Computational Physics*, 14 (3), November, pp. 227–253.

[2] Nitikitpaiboon, C., and Bathe, K., 1993. "An Arbitrary Lagrangian-Eulerian velocity potential formulation for fluid-structure interaction". *Computers and Structures*, 47 (5), pp. 871–891.

[3] Gilmanov, A., and Acharya, S., 2008. "A hybrid immersed boundary and material point method for simulating 3D fluid-structure interaction problems".*International Journal for Numerical Methods in Fluids*, 56, August, pp. 151–177.

[4] Huang, W., Chang, C., and Sung, H., 2011. "An improved penalty immersed boundary method for fluid-flexible body interaction".*Journal of Computational Physics*, 230, March, pp.5061–5079.

[5] Wang, X., and Zhang, L., 2010. "Interpolation functions in the immersed boundary and finite element methods".*ComputMech*, 45, pp. 321–334.

[6] Wang, X., Wang C., and Zhang, L., 2012. "Semi-implicit formulation of the immersed finite element method".*ComputMech*, 49, October, pp. 421–430.

[7] Glowinski, R., Pan, T., Hesla, T., Joseph, D., and Periaux, J., 2001. "A fictitious domain approach to the direct numerical simulation of incompressible viscous flow past moving rigid bodies: application to particulate flow". *Journal of Computational Physics*, 169, April, pp. 363–426.

[8] Sugiyama, K., Ii, S., Takeuchi, S., Takagi, S., and Matsumoto, Y., 2010. "Full Eulerian simulation of biconcave neo-Hookean particles in a Poiseuille flow". *Journal of ComputMech*, 46, March, pp. 147–157.

[9] Sugiyama, K., Ii, S., Takeuchi, S., Takagi, S., and Matsumoto, Y., 2011. "A full Eulerian finite difference approach for solving fluid-structure coupling problems". *Journal of Computational Physics*, 230, October, pp. 596–627

[10]Ii, S., Sugiyama, K., Takeuchi, S., Takagi, S., and Matsumoto, Y., 2011. "An implicit full Eulerian method for the fluid-structure interaction problem". *International Journal for Numerical Methods in Fluids*, 65,October, pp. 150–165

[11]Sugiyama, K., Nagano, N., Takeuchi, S., Ii, S., Takagi, S., and Matsumoto, Y., 2011. "Particle-in-cell method for fluid-structure interaction simulations of neo-Hookean".*Theoretical and Applied Mechanics*, 59, October, pp. 245–256.

[12]Ii, S., Gong, X., Sugiyama, K., Wu, J., Huang, H., and Takagi, S., 2011. "A full Eulerian fluid-membrane coupling method with a smoothed volume of fluid approach". *Journal of Computational Physics*, 69, December, pp. 1–33.

[13]Takagi, S., Sugiyama, K., Ii, S., and Matsumoto, Y., 2012. "A review of full Eulerian methods for fluid structure interaction problems". *Journal of Applied Mechanics*, 79, September, pp. 1–18.

[14]Ii, S., Sugiyama, K., Takagi, S., and Matsumoto, Y., 2012. "A computational blood flow analysis in a capillary vessel including multiple red blood cells and platelets". *Journal of Biomechanical Science and Engineering*, 7 (1), November, pp. 72–83.

[15]Youngs, D.L., 1984. "An interface tracking method for a 3D Eulerian hydrodynamics code". *Technical Report* 44/92/35, AWRE.

[16]Mirzaii, I., and Passandideh-Fard, M., 2012. "Modeling free surface flows in presence of an arbitrary moving object". *International Journal of Multiphase Flow*, 39, October, pp. 216–226.

[17]Marckmann, G., and Verron, E., 2006. "Comparison of hyperelastic models for rubber-like materials". *Rubber Chemistry and Technology*, 79, November, pp. 835–858.

[18]Robinson, A., Schroeder, C., and Fedkiw, R., 2011. "A symmetric positive definite formulation for monolithic fluid structure interaction". *Journal of Computational Physics*, 230, November, pp. 1547-156.